🔓 **Open Access**

# Surface Plasmon Resonance Sensor Based on a Novel D-Shaped Photonic Crystal Fiber for Low Refractive Index Detection

**Xin Chen**
**Li Xia**
**Chen Li**

◆ **IEEE**

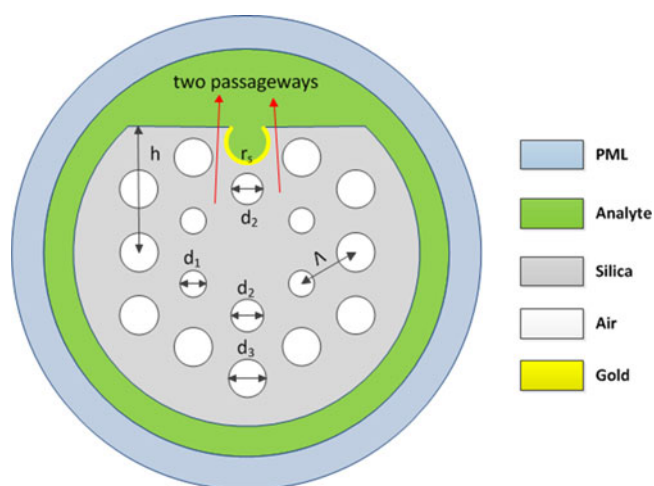# Surface Plasmon Resonance Sensor Based on a Novel D-Shaped Photonic Crystal Fiber for Low Refractive Index Detection

**Xin Chen** [ID], **Li Xia** [ID]**, and Chen Li**

School of Optical and Electronic Information, Huazhong University of Science and Technology, Wuhan 430074, China

**Abstract:**  A novel D-shaped photonic crystal fiber refractive index sensor based on surface plasmon resonance (SPR) is proposed and numerically studied. Different from the normal D-shaped structures, we here used an open-ring channel coated with gold film to excite the plamonic modes. The coupling properties and sensing performance of this structure are analyzed using finite element method. Simulation results indicate that the sensor has a sensing range from 1.20 to 1.29. When the analyte refractive index (RI) is above 1.25, the anti-crossing effect starts to appear, and the peak loss of the loss spectra remains nearly constant with increasing RI. The maximum spectral sensitivity of 11055 nm/RIU and high resolution of $9.05 \times 10^{-6}$ RIU can be obtained at 1.29. For the purpose of optimizing sensing performance, the effects of the structure parameters on the resonant spectra are also studied. The excellent sensing performance makes the proposed SPR sensor a competitive candidate in low refractive index detection applications.

**Index Terms:** Surface plasmon resonance, photonic crystal fiber, refractive index measurement, finite element method.

## 1. Introduction

Surface Plasmon Resonance (SPR) is a prominent optical phenomenon that arises as the extent of energy transfer from photons to surface plasmon waves under appropriate conditions [1]. This optical effect, owing to its high sensitivity, real-time and label-free monitoring, has already been extensively studied and applied to applications like medical diagnostics, solution concentration measurement, environment monitoring, and biochemistry research [2]–[5]. Nowadays, most of the commercial SPR sensors are based on attenuated total reflection (ATR) principle and adopt prism structures. These sensing devices have a high demand of optical and mechanical components, which results in a bulky measurement platform and an expensive equipment cost. To solve this problem, the first fiber-based SPR sensor was proposed and demonstrated by Jorgenson in 1993 [6]. Since then, numerous SPR fiber sensors based on simulation and experimental results have been reported.
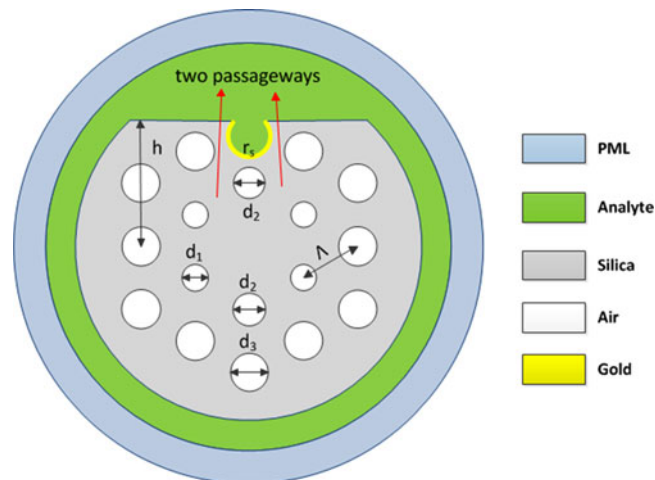
Fig. 1. Schematic illustration of the proposed D-shaped PCF sensor.

So far, there are various fiber types that have been reported in SPR fiber sensing technology, such as single-mode fibers (SMF) [7], multimode fibers (MMF) [8], and photonic crystal fibers (PCF) [9]–[11]. PCF in particular, has attracted more attention, as it provides a perfect solution to the phase matching and packing issues in the SPR sensing [12]. However, in conventional PCF based sensing structures, the analyte is selectively filled into the air holes and then coated with metal film. These procedures are very difficult and time-consuming to some extent. Thus for the purpose of eliminating these limitations, D-shaped PCF SPR sensors are widely investigated. Tian *et al.* proposed an all-solid D-shaped PCF sensor with a sensing range of 1.33–1.38 and a sensitivity larger than 7300 nm/RIU [13]. An *et al.* reported a D-shaped PCF SPR sensor with gold plated on the polished plane. The detection range of analyte RI is 1.33–1.38, and the maximum sensitivity of 10,493 nm/RIU is obtained at 1.38 [14]. Dash *et al.* described a Graphene-Based D-shaped PCF SPR biosensor with a spectral sensitivity of 3700 nm/RIU [15]. In spite of the promising results researchers have achieved, most of these sensing structures can only detect analyte with RI higher than 1.30. In other words, the investigation on D-shaped PCF SPR sensor with lower RI detection range is still lacking. As a matter of fact, the RI of many halogenated ethers and pharmaceuticals are located in the lower RI range. For example, sevoflurane has a RI about 1.27 and serves as the anesthetic in the medical area. Therefore, the sensors with lower RI detection range may have the potential applications like pharmaceutical inspection and pharmaceutical leakage monitoring.

In this work, we present a high sensitivity SPR sensor based on a novel D-shaped PCF structure. The open-ring channel coated with gold film can not only reduce the coating area and simplify the fabrication process, but also create two passageways to enhance the resonance effect and improve the sensitivity. Numerical results exhibit a maximum spectral sensitivity of 11,055 nm/RIU and a high resolution of $9.05 \times 10^{-6}$ RIU when analyte RI is 1.29. The sensing range of this sensor is from 1.20 to 1.29, and the anti-crossing effect starts to appear when analyte RI is higher than 1.25. The working wavelength of this fiber sensor is at mid-infrared region, which is determined by the fiber structure parameters and the materials we used. We believe our studies can provide a feasible structure for applications based on low RI measurement.

## 2. Sensor Design and Numerical Modeling

The Schematic illustration of our proposed D-shaped PCF is shown in Fig. 1. This structure has two hexagonal rings: the inner ring consists of air holes with two different diameters, $d_1 = 1.2 \ \mu$m and $d_2 = 1.5 \ \mu$m; while the diameter of outer layer air holes is fixed at $d_3 = 1.8 \ \mu$m. The hole-to-hole pitch is $\Lambda = 3 \ \mu$m, and the radii of the PCF is set to be 2.75$\Lambda$. In order to excite the surface
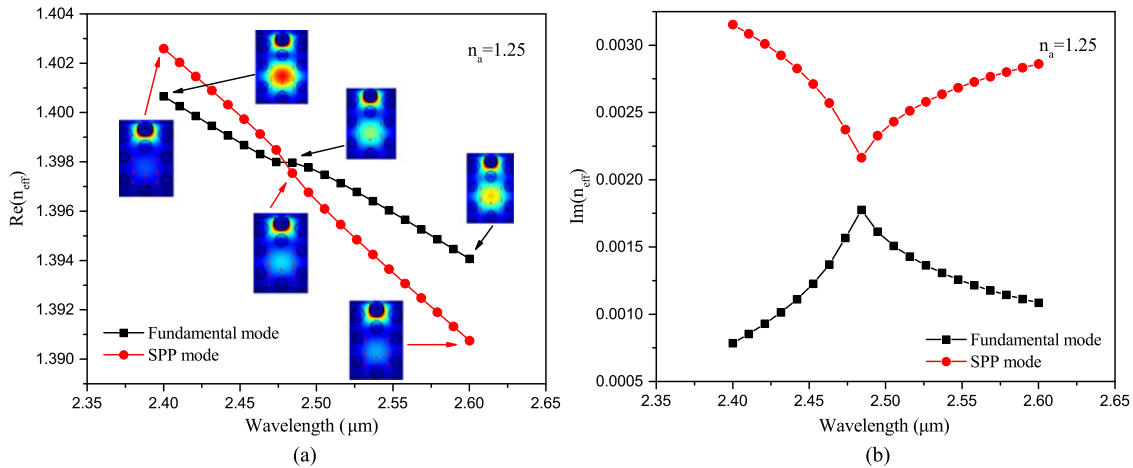
Fig. 2. Real part (a) and imaginary part (b) of the effective index as a function of incident wavelength when analyte RI = 1.25. The inserts are electric field distributions of these two modes at specific wavelengths. The red arrows in the inserts indicate the electric field direction.

plasmon, a thin gold film with thickness $t = 50$ nm is deposited on the inner surface of the open-ring analyte channel. The analyte can flow through this channel and filter some impurities larger than the opening. In addition, two passageways are created by this channel, thus according to [16], the coupling between optical and plasmonic modes can be enhanced due to the promoted energy leakage from the fiber core. The radii and the center location of this open-ring channel are $r_s = 1$ $\mu$m and $y = h - 0.75 r_s$ respectively, where $h = 6$ $\mu$m is the distance between the D-shaped section and fiber core.

In this fiber, the D-shaped structure can be fabricated using stack-and-draw method and side polishing technique, the gold film can be coated with a chemical deposition technique [17]. In our simulation, the background material of proposed PCF is fused silica, and its refractive index is determined by Sellmeier equation [18]. Furthermore, the dielectric constant of gold is defined by Drude model, which can be expressed as [19]

$$\varepsilon(\omega) = \varepsilon_1 + i\varepsilon_2 = \varepsilon_\infty - \frac{\omega_p^2}{\omega(\omega + i\omega_c)} \tag{1}$$

Where $\varepsilon_\infty = 9.75$ is the dielectric constant of gold at high frequencies, $\omega_p = 1.36 \times 10^{16}$ is the plasma frequency, $\omega_c = 1.45 \times 10^{14}$ is the scattering frequency of electrons, and $\omega$ is the angular frequency of the incident light [14].

The confinement loss of this sensor can be expressed as [14]:

$$\alpha_{loss} = 8.686 \times \frac{2\pi}{\lambda} \text{Im}\left(n_{eff}\right) \times 10^4 \text{ (dB/cm)} \tag{2}$$

Where $\lambda$ is the wavelength in micrometer of incident light, and $\text{Im}(n_{eff})$ is the imaginary part of the effective refractive index. For the purpose of accurate calculation, a perfect matched layer (PML) is introduced in the calculation zone edges to absorb radiation energy [20]. The simulation process is accomplished by the commercial finite element method solver–COMSOL Multiphysics.

## 3. Results and Discussion

Fig. 2 (a) and (b) illustrate the dispersion relations of plasmonic mode (or surface plasmon-polaritons (SPP) mode in other words) and fundamental mode when analyte RI $n_a = 1.25$. The black curve stands for fundamental mode, while the red curve represents the plasmonic mode. The inserts in Fig. 2(a) are the electric field distributions of both two modes at specific wavelengths. The red
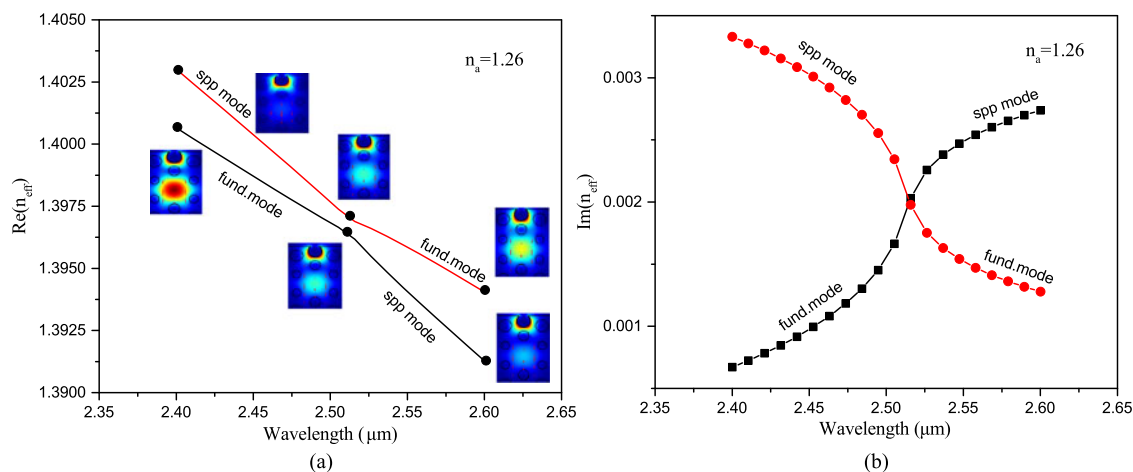
Fig. 3. Real part (a) and imaginary part (b) of the effective index as a function of incident wavelength when anti-crossing effect happens. The analyte RI is 1.26 and the inserts are electric field distributions of coupled modes at specific wavelengths. The red arrows in the inserts indicate the electric field direction.

arrows in the inserts indicate the electric field direction. As shown in these pictures, a strong SPR effect occurs at 2.48 $\mu$m, where the real parts of effective index (Re($n_{eff}$)) of both two modes coincide with each other, and an obvious peak appears on the loss spectra (as the confinement loss is proportional to the imaginary part of effective index Im($n_{eff}$)). A maximum energy transfers from the fundamental mode to the plasmonic mode at the resonant wavelength. Furthermore, we should notice that the coupling between fundamental and plasmonic modes is incomplete, as they share different Im($n_{eff}$) value and the anti-crossing effect did not happen.

Although the coupling between fundamental and plasmonic modes is not complete when $n_a \leq$ 1.25, we find that things will be very different at larger $n_a$. Fig. 3 exhibits the dispersion relations of fundamental (black line) and plasmonic modes (red line) when $n_a = 1.26$. Fig. 3 (a) and (b) are the real part and imaginary part of the effective index as a function of incident wavelength. The inserts in Fig. 3(a) are the electric field distribution variations with increasing wavelength, and can illustrate the anti-crossing effect vividly.

As shown in Fig. 3(a), the coupling between two modes happens near the anti-crossing point, which is 2.51 $\mu$m here, and then these two modes will split into two new modes at longer wavelength. According to Ref. [12], when the incident wavelength is far shorter than the anti-crossing point, the energy of fundamental mode is well-confined in the fiber core. As the wavelength increases, the coupling between plasmonic and fundamental modes starts to appear. When wavelength reaches the anti-crossing point, we should notice that the electric field distribution of fundamental and plasmonic modes are almost the same, and the Re($n_{eff}$) of both two modes experienced a sudden change. As the wavelength continues to increase, the energy of fundamental mode is thoroughly transferred into plasmonic mode, while the energy transition of plasmonic mode is quite the contrary. This completely energy transfer can also be reflected from Fig. 3(b). For the black curve, the Im($n_{eff}$) follows the fundamental mode part before the anti-crossing point, and switches to plasmonic mode part after the anti-crossing point. Different from the coupling phenomena in Fig. 2, the curves in Fig. 3(b) do intersect with each other at the anti-crossing point, therefore the coupling between these two modes is complete.

For the purpose of optimizing sensing performance, the effects of the structure parameters on the resonant spectra are systemically investigated. Fig. 4 depicts the variations of loss spectra with different inner air hole diameters $d_1$ (a) and $d_2$ (b), different outer air hole diameter $d_3$ (c), and different pitch size $\Lambda$ (d). The RI of analyte is set to be $n_a = 1.26$. As shown in Fig. 4(a), the resonance peak shifts to longer wavelength with increasing $d_1$, and the coupling between the two
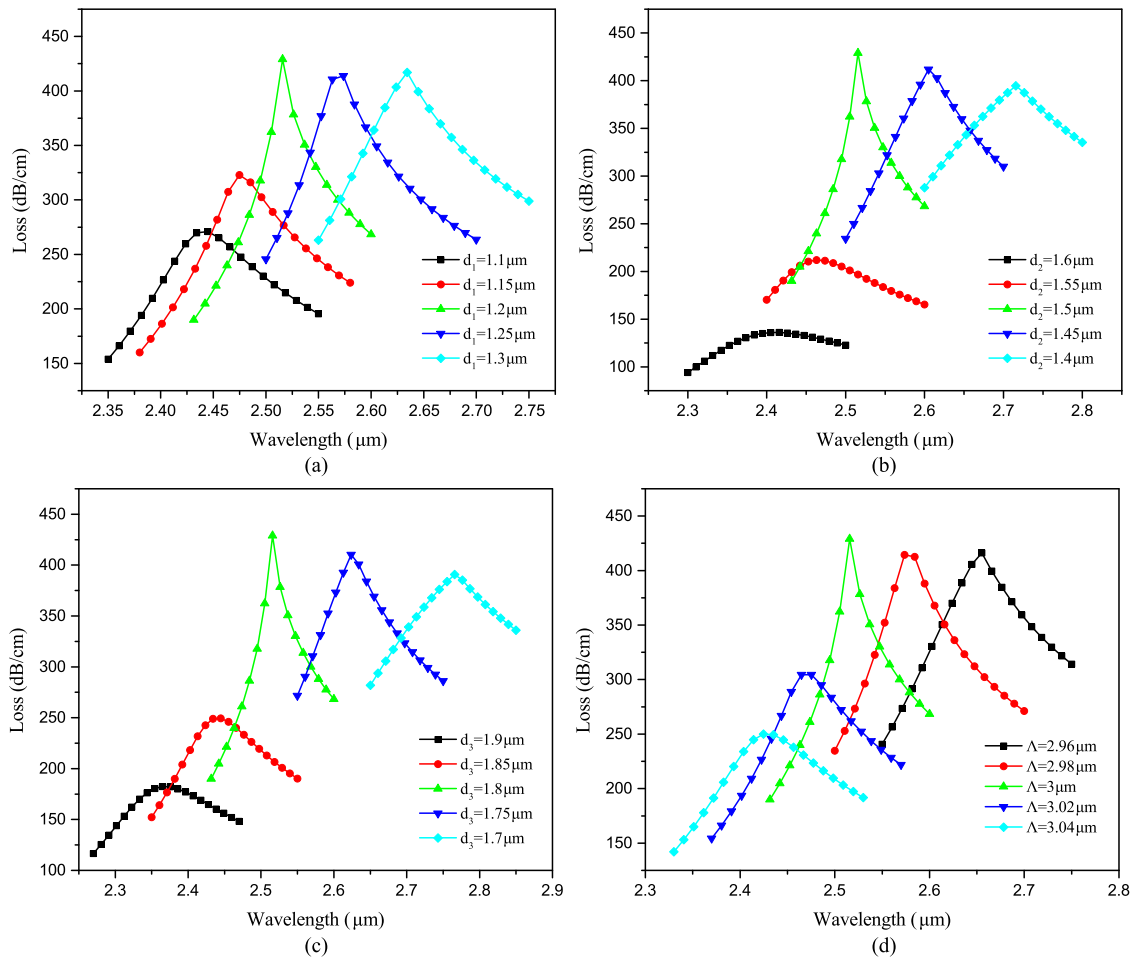
Fig. 4. Loss curves of the proposed SPR-PCF sensor for different inner layer hole diameters $d_1$ (a) and $d_2$ (b), different outer layer hole diameters $d_3$ (c) and different pitch size $\Lambda$ (d).

modes gradually changes from incomplete transition ($d_1 = 1.1$–$1.2$ $\mu$m) to complete transition ($d_1 = 1.2$–$1.3$ $\mu$m).

For the incomplete coupling part ($d_1 = 1.1$–$1.2$ $\mu$m), these larger sized inner holes lead to a smaller Re($n_{\text{eff}}$) value of fundamental mode and an enhanced coupling in the PCF sensor, which finally result in a red shift (under phase matching condition) and an increased resonant peak loss of the loss spectrum. For the complete coupling part ($d_1 = 1.2$–$1.3$ $\mu$m), when $d_1$ increases, the core confinement ability begins to increase, thus a smaller Im($n_{\text{eff}}$) value of the fundamental mode is obtained at the original resonant wavelength. By noting that the anti-crossing effect happens when the Im($n_{\text{eff}}$) values are equal for both fundamental and plasmonic modes (loss matching condition), we can easily deduce that the anti-crossing point will have a red shift with increasing $d_1$.

In Fig. 4 (b) and (c), a red shift of loss spectra is observed as $d_2$ or $d_3$ decreases. Similarly, it can be explained by the fact that smaller sized air holes surrounding the open-ring channel make a bigger effective index of plasmonic mode, which finally leads to the red shift in the loss spectra under phase/loss matching condition. Fig. 4(d) shows the $\Lambda$-dependent loss properties. When $\Lambda$ decreases, the loss spectra also experience a red shift, as the effective index of fundamental mode decreases and that of the plasmonic mode start to increase.

The thickness of gold film has a large impact on the sensing performance. If the gold film is too thick, the sensitivity and the peak loss will be significantly reduced, as the electric field cannot
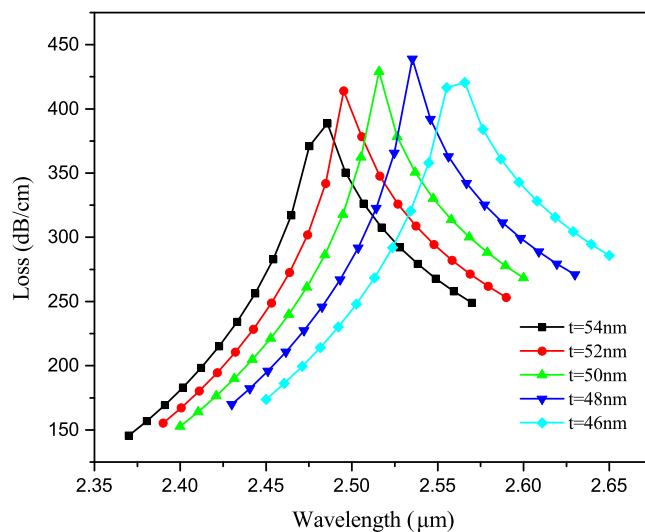
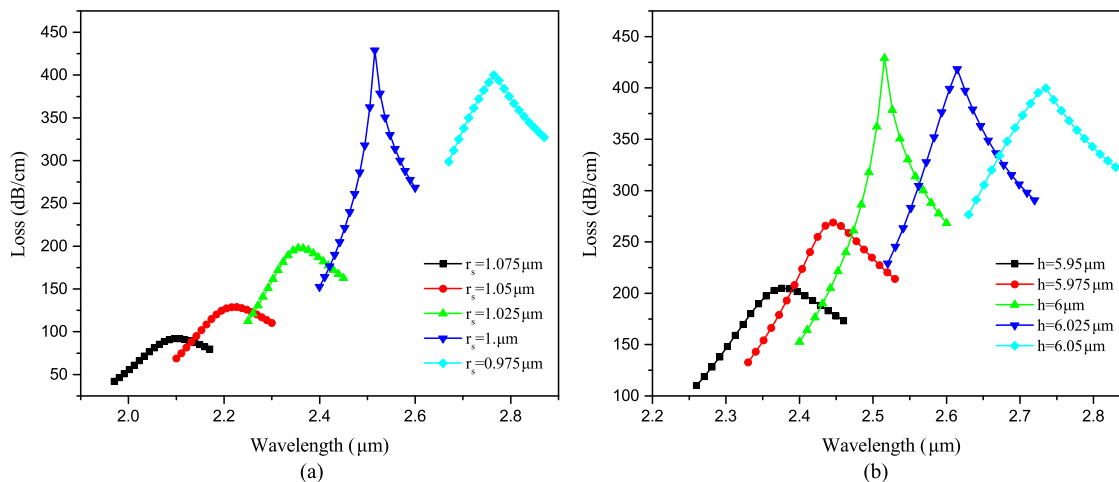Fig. 5. Loss curves of the proposed SPR-PCF sensor for different gold film thickness $t$.



Fig. 6. Loss curves of the proposed SPR-PCF sensor for different radii $r_s$ (a) and different D-section distance $h$ (b) of the open-ring channel.

penetrate through the gold layer. While if the gold film is too thin, the plasmonic wave will be strongly damped because of radiation damping. Fig. 5 exhibits the loss spectra variations for different gold film thickness $t$ ranging from 46 nm to 54 nm. As is shown, the loss spectrum moves towards longer wavelength from 2.48 $\mu$m to 2.56 $\mu$m with $t$ decreasing from 54 nm to 46 nm. A similar phenomenon was also noted in [21], [22]. In addition, the resonance intensity increases when $t$ changes from 54 nm to 48 nm. Since the gold film is coated on the inner surface of the open-ring channel, more energy is transferred to the plasmonic modes when $t = 48$ nm resulting in the highest peak loss. And we can also notice that the loss spectra of $t = 48$ nm has a sharper resonance peak, thus $t = 48$ nm might be an optimized gold film thickness.

Fig. 6(a) and (b) show the loss curves for different radii $r_s$ and different D-section distance $h$ of the open-ring channel. We find these two structure parameters have significant effects on the resonant spectra. With slightly increase in $r_s$, the Re($n_{eff}$) of fundamental mode increases while that of the plasmonic mode drops rapidly, besides the resonance intensity is remarkably weakened. Thus in Fig. 6(a), the loss curves exhibit a blue shift and a decreased peak loss with increasing $r_s$. However,
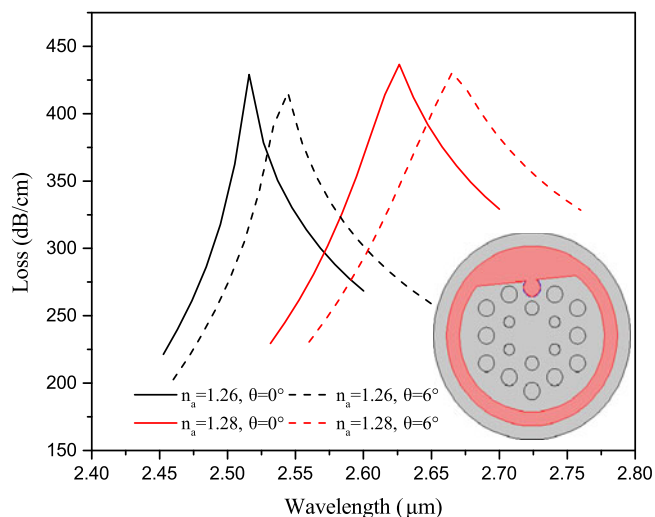
Fig. 7. Loss curves of the proposed SPR-PCF sensor for different polished plane inclination.
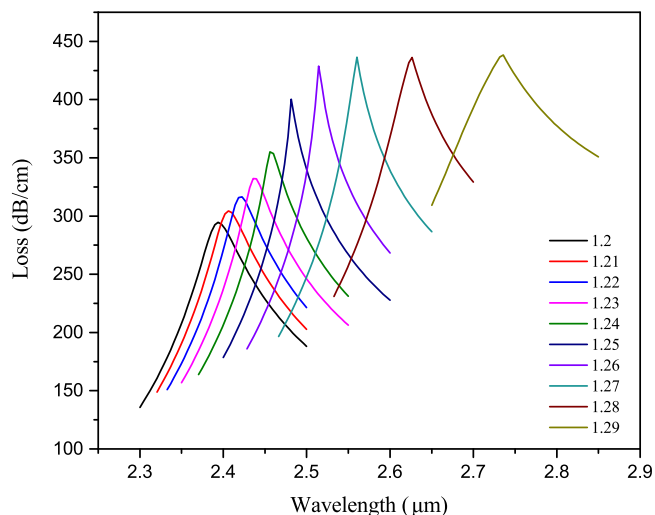


Fig. 8. Loss curves of the proposed SPR-PCF sensor for different analyte RI.

as the distance between D-section and the fiber core $h$ increases, the loss spectrum shows a red shift and an enhanced coupling in Fig. 6(b). This can also be explained by the changes occurred in effective index of the plasmonic mode.

Fig. 7 shows the impact of the polished plane inclination on fiber sensing performance. We find that the changes in inclination of the polished plane have little influence on the loss spectra and the sensitivity. With the inclination changing from 0° to 6°, the loss spectrum only shifts about 30 nm when $n_a = 1.26$, and 39 nm when $n_a = 1.28$. Besides, when the inclination is within 4°, the changes in loss spectra are hard to recognize. This phenomenon can be explained by that the changes of polished plane inclination have little effect on the plasmonic structure, as the gold film is deposited on the inner surface of the open-ring analyte channel. In that case, the production requirement of this sensor is reduced.

The loss curves of our proposed SPR-PCF for different RI of analyte (ranging from 1.2 to 1.29) is shown in Fig. 8. With the increase of $n_a$, the resonance wavelength experiences a red shift, and the coupling between plasmonic and fundamental modes changes from incomplete to complete
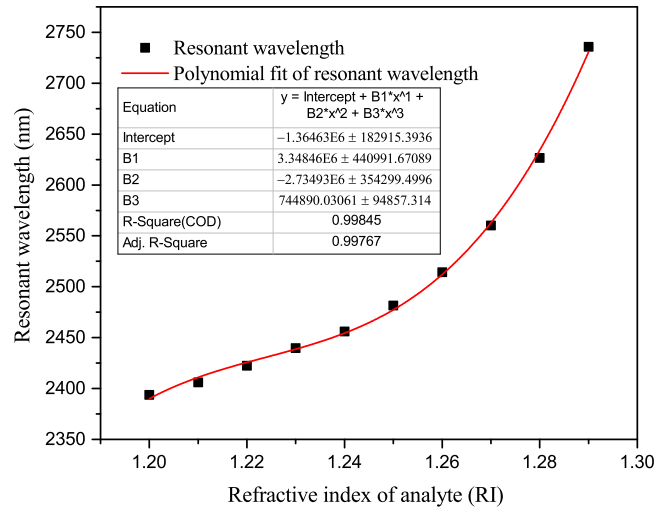
Fig. 9. Variations of resonance wavelength with analyte RI changing from 1.20 to 1.29. The insert table is the results of polynomial fitting.

transition. It should be noted that when $n_a \geq 1.26$, the anti-crossing effect appears, and the peak loss of the loss spectra remains nearly constant with increasing $n_a$. This can be explained by the fact that the losses of the plasmonic and fundamental modes vary contrarily with increasing $n_a$. Through the shift of resonant wavelength, we can characterize the wavelength sensitivity of our proposed PCF sensor. The sensitivity can be expressed as follows [14]:

$$S_\lambda(\text{nm/RIU}) = \frac{\triangle \lambda_{\text{peak}}}{\triangle n_a} \qquad (3)$$

Where $\triangle \lambda_{\text{peak}}$ is the shift of the resonant wavelength, and $\triangle n_a$ refers to the variation of the analyte RI.

The resonant wavelength variations with analyte RI changing from 1.20 to 1.29 are shown in Fig. 9. The insert table shows the polynomial fitting results, and the slope of this fit curve stands for the sensitivity of our proposed SPR-PCF sensor. The adjusted R-square value of this fitting is 0.99767, suggesting a great fitting agreement. With the increase of $n_a$, the resonant point is moving to longer wavelength, and a maximum spectral sensitivity of 11,055 nm/RIU is achieved when $n_a = 1.29$. The refractive index of resolution is defined as:

$$R = \triangle n_a \triangle \lambda_{\text{min}} / \triangle \lambda_{\text{peak}} \qquad (4)$$

Where $\triangle \lambda_{\text{min}}$ is the minimum spectral resolution assumed to be 0.1 nm. A high resolution of $9.05 \times 10^{-6}$ RIU is obtained at 1.29 in the proposed structure.

In summary, the proposed sensor exhibits a higher sensitivity of 11,055 nm/RIU and a better resolution of $9.05 \times 10^{-6}$ compared with the normal D-shaped structures [14], [15]. The sensing range of this sensor is 1.20–1.29, which makes it more competitive in the measurement of low RI range. The coupling between plasmonic and fundamental mode is enhanced, as two passageways created by the open-ring channel can promote the energy leakage from the fiber core [16]. And the anti-crossing effect appears when analyte RI is higher than 1.25.

## 4. Conclusion

In this work, a novel D-shaped PCF sensor based on SPR effect is present and numerically investigated. Different from the normal D-shaped structures, the SPR effect is excited by coating thin gold film on the open-ring channel, which can enhance the resonance effect and improve the spectral sensitivity of proposed sensor. In addition, the usage of this channel can reduce the coating

area of gold film, thus makes the fabrication process more simplified and cost-effective. Simulation results show that the sensor we proposed can detect low refractive index ranging from 1.20 to 1.29 with high spectral sensitivity. On account of the promising sensing results, the low refractive index sensing range and the simple compact fiber design, the proposed SPR sensor can be a competitive candidate in low refractive index detection applications.

## References

[1] D. J. J. Hu and H. P. Ho, "Recent advances in plasmonic photonic crystal fibers: Design, fabrication and applications," *Adv. Opt. Photon.*, vol. 9, no. 2, pp. 257–314, Jun. 2017.

[2] B. Lee, S. Roh, and J. Park, "Current status of micro- and nano-structured optical fiber sensors," *Opt. Fiber Technol.*, vol. 15, no. 3, pp. 209–221, 2009.

[3] L. Xing, Y. Zheng, Y. Sun, M. Wang, H. Cui, and T. Li, "Optical fiber sensor determination of the water salinity based on surface plasmon resonance," *Infrared Laser Eng.*, vol. 44, no. 4, 2015, Art. no. 1290.

[4] J. Homola, S. S. Yee, and G. Gauglitz, "Surface plasmon resonance sensors: Review," *Sens. Actuators B, Chem.*, vol. 54, no. 1, pp. 3–15, 1999.

[5] B. Gupta and R. Verma, "Surface plasmon resonance-based fiber optic sensors: Principle, probe designs, and some applications," *J. Sens.*, vol. 2009, Jul. 2009, Art. no. 979761.

[6] R. Jorgenson and S. Yee, "A fiber-optic chemical sensor based on surface plasmon resonance," *Sens. Actuators B, Chem.*, vol. 12, no. 3, pp. 213–220, 1993.

[7] R. Slavík, J. Homola, and J. Ctyroký, "Single-mode optical fiber surface plasmon resonance sensor," *Sens. Actuators B, Chem.*, vol. 54, no. 1, pp. 74–79, 1999.

[8] A. Trouillet, C. Ronot-Trioli, C. Veillas, and H. Gagnaire, "Chemical sensing by surface plasmon resonance in a multimode optical fibre," *Pure Appl. Opt., J. Eur. Opt. Soc. Part A*, vol. 5, no. 2, pp. 227–237, 1996.

[9] B. Shuai, L. Xia, and D. Liu, "Coexistence of positive and negative refractive index sensitivity in the liquid-core photonic crystal fiber based plasmonic sensor," *Opt. Exp.*, vol. 20, no. 23, pp. 25858–25866, Nov. 2012.

[10] Y. Zhao, Z. Deng, and J. Li, "Photonic crystal fiber based surface plasmon resonance chemical sensors," *Sens. Actuators B, Chem.*, vol. 202, Suppl. C, pp. 557–567, 2014.

[11] Y. Han, L. Xia, and D. Liu, "Highly sensitive fiber refractive index sensor based on side-core holey structure," *Chin. Phys. B*, vol. 23, no. 10, 2014, Art. no. 104219.

[12] B. Shuai, L. Xia, Y. Zhang, and D. Liu, "A multi-core holey fiber based plasmonic sensor with large detection range and high linearity," *Opt. Exp.*, vol. 20, no. 6, pp. 5974–5986, Mar. 2012.

[13] M. Tian, P. Lu, L. Chen, C. Lv, and D. Liu, "All-solid d-shaped photonic fiber sensor based on surface plasmon resonance," *Opt. Commun.*, vol. 285, no. 6, pp. 1550–1554, 2012.

[14] G. An, X. Hao, S. Li, X. Yan, and X. Zhang, "D-shaped photonic crystal fiber refractive index sensor based on surface plasmon resonance," *Appl. Opt.*, vol. 56, no. 24, pp. 6988–6992, Aug. 2017.

[15] J. N. Dash and R. Jha, "On the performance of graphene-based d-shaped photonic crystal fibre biosensor using surface plasmon resonance," *Plasmonics*, vol. 10, no. 5, pp. 1123–1131, Oct. 2015.

[16] G. Wang *et al.*, "Highly sensitive d-shaped photonic crystal fiber biological sensors based on surface plasmon resonance," *Opt. Quantum Electron.*, vol. 48, pp. 1–9, Dec. 2016.

[17] J. Boehm, A. François, H. Ebendorff-Heidepriem, and T. M. Monro, "Chemical deposition of silver for the fabrication of surface plasmon microstructured optical fibre sensors," *Plasmonics*, vol. 6, no. 1, pp. 133–136, Mar. 2011.

[18] F. Wang, Z. Sun, C. Liu, T. Sun, and P. K. Chu, "A highly sensitive dual-core photonic crystal fiber based on a surface plasmon resonance biosensor with silver-graphene layer," *Plasmonics*, vol. 12, pp. 1–7, Dec. 2016.

[19] C. Du, Q. Wang, H. Hu, and Y. Zhao, "Highly sensitive refractive index sensor based on four-hole grapefruit microstructured fiber with surface plasmon resonance," *Plasmonics*, vol. 12, no. 6, pp. 1961–1965, Dec. 2017.

[20] X. Yang, Y. Lu, L. Duan, B. Liu, and J. Yao, "Temperature sensor based on hollow fiber filled with graphene-ag composite nanowire and liquid," *Plasmonics*, vol. 12, no. 6, pp. 1805–1811, Dec. 2017.

[21] J. Xue, S. Li, Y. Xiao, W. Qin, X. Xin, and X. Zhu, "Polarization filter characters of the gold-coated and the liquid filled photonic crystal fiber based on surface plasmon resonance," *Opt. Exp.*, vol. 21, no. 11, pp. 13733–13740, Jun 2013.

[22] C. Liu *et al.*, "Mid-infrared surface plasmon resonance sensor based on photonic crystal fibers," *Opt. Exp.*, vol. 25, no. 13, pp. 14227–14237, Jun. 2017.